Available online at www.sciencedirect.com
SCIENCE DIRECT®
Acta Materialia 53 (2005) 2607–2616
Acta MATERIALIA
www.actamat-journals.com

Microstructure control and ductility improvement of La–Al–(Cu, Ni) composites by Bridgman solidification

Y. Zhang [a,c,*], W. Xu [b], H. Tan [b], Y. Li [a,b]

[a] Advanced Materials for Micro- & Nano-Systems, Singapore-MIT Alliance, National University of Singapore, Singapore 117576, Singapore
[b] Department of Materials Science, National University of Singapore, Singapore 119260, Singapore
[c] State Key Laboratory for Advanced Metals and Materials, University of Science and Technology Beijing, Xue Yuan Road 30, HaiDian District, Beijing 100083, China

Received 22 December 2004; received in revised form 22 December 2004; accepted 9 February 2005
Available online 2 April 2005

Abstract

Microstructure evolutions were experimentally studied as a function of growth velocity and alloy composition in $La_xAl_{14}(Cu, Ni)_{86-x}$ alloys ($x = 57$–74). The composition–velocity ranges were determined for the formation of eutectic, amorphous, eutectic + compound, amorphous + dendrite, and eutectic + dendrite. A skewed eutectic coupled zone was found towards the compound phase. A composite structure composed of ductile La dendrites in a matrix of either eutectic or amorphous phase can be produced in hypoeutectic alloys. Compressive tests were performed on amorphous/dendrite and eutectic/dendrite composites. As the volume fraction of dendrites increases, fracture strength linearly decreases and obeys a rule-of-mixtures relationship, whereas plastic strain exhibits an exponential increase. Optimised mechanical properties can be realized through both alloy composition design and well-controlled solidification processing.

Keywords: Bulk metallic glass; Bridgman solidification; Eutectic; Composite; La based alloy

1. Introduction

Over the past few decades, bulk metallic glasses (BMGs) produced at low cooling rates have been extensively explored owing to their fundamental scientific importance and engineering application potential [1–5]. In terms of mechanical properties, BMGs have been reported to have advantages over conventional metallic alloys, in terms of higher strength, larger elastic strain limit, higher hardness and better wear resistance [2,4]. However, at room temperature monolithic BMGs have exhibited inhomogeneous plastic deformation behavior without strain hardening, during which all the plastic flow is confined in the localized regions of a few shear bands and eventually leads to catastrophic failure with little plastic strain [2,4]. To improve the ductility of BMGs, more attempts have been recently made to introduce in situ ductile crystalline phases into the amorphous matrix [6–11]. For instance, the introduction of the ductile Ta-rich solid solution particles dramatically enhanced the compressive plastic strain to be about 17% with yield strength of 1700 MPa in a Be-free $(Zr_{70}Ni_{10}Cu_{20})_{82}Ta_8Al_{10}$ alloy [9]. In a Ti-based $Ti_{50}Cu_{23}Ni_{20}Sn_7$ bulk metallic glass composite, the formation of ductile hexagonal close-packed Ti dendrites resulted in up to 6% compressive plastic strain as well as yield strength of 1190 MPa [10].

Usually, control and improvement of mechanical properties for bulk metallic glass composites can be realized by means of microstructure control, i.e., appropri-

* Corresponding author. Tel.: +86 106 233 4333; fax: +86 106 233 2508.
E-mail address: drzhangy@skl.ustb.edu.cn (Y. Zhang).

1359-6454/$30.00
doi:10.1016/j.actamat.2005.02.020

ate design of alloy composition and well-controlled solidification processing. The appropriate design of alloy composition is of great importance in producing bulk metallic glass composites with desired microstructures. In a previous study on the La–Al–Cu–Ni multicomponent alloy system [12], the optimum glass forming ability was found to occur at an off-eutectic composition, which was proposed to be related to a skewed eutectic coupled zone. In addition to alloy design, well-controlled solidification has played a very significant role in achieving a bulk metallic glass composite with optimized mechanical properties. Until now, the most frequently used technique to prepare amorphous/dendrite composites has been copper mould casting. However, for mm-sized samples the resultant microstructures are inhomogeneous along the radius for rods, since different cooling rates are produced from the outer surface to the center. A ring-shaped alloy sample is therefore obtained, which may lead to a deviation of characterization of mechanical properties. In order to gain more insight into the microstructural development of bulk metallic glass composite and to achieve a uniform composite structure, Bridgman directional solidification was employed in the present study on La–Al–Cu–Ni multi-component alloys. The resultant mechanical properties were also characterized.

2. Experimental procedures

The ingots were prepared by arc-melting a mixture of pure La (99.9%), Al (99.9%), Ni (99.98%) and Cu (99.999%) in an argon atmosphere. The composition $La_xAl_{14}(Cu,Ni)_{86-x}$ is nominally expressed in atomic per cent, and the alloys were designated as L57, L59, L61, L62, L64, L66, L68, L72, and L74 for simplicity. Each master ingot was first melted five times, and then crushed, and remelted four times. Bridgman solidification was carried out by induction melting of the alloys in the vacuum sealed quartz tubes with 3 mm internal diameter and a wall thickness of 1 mm. The alloys were then remelted at 923 K and kept for 20 min, and subsequently withdrawn at constant growth velocities (V) in the range of 0.008–4.8 mm/s through a temperature gradient (G) of 15 K/mm into a water bath. The cooling rate (R) can be calculated as $R = GV$.

The rod samples with 3 mm diameter were mounted and polished for characterization under a scanning electron microscope (SEM) and optical microscopy (OM). An image analyzer with Leica Qwin image processing and analysis system was used to measure the volume fraction of the dendritic phase. Phase identification was carried out by a Philips X'Pert-MPD system with Cu Kα radiation of wavelength 0.154056 nm. Differential scanning calorimetry (DSC) was used to analyze the thermal properties of solidified samples at a heating rate of 40 K/min.

An Instron-5500R mechanical testing equipment was used to perform the compression test. The cylindrical samples with length of 6 mm were cut by a diamond cutter and the ends of the specimens were mechanically polished. For each type of sample, three or four specimens were tested. Strain gauges (Gauge type is FLA-05-11) were attached to the surface of the specimens to obtain one-dimensional local strains. Compressions were conducted using constant crosshead velocity of 0.06 mm/min. The resultant strain rate was $1.67 \times 10^{-4}\ s^{-1}$.

3. Results

3.1. Microstructure evolution

$La_xAl_{14}(Cu,Ni)_{86-x}$ alloys were studied by Bridgman solidification at growth velocities (V) ranging from 0.008 to 4.8 mm/s. The solidified samples have exhibited uniform microstructures throughout the transverse sections (Fig. 1). The resultant microstructures are summarized in Table 1 as a function of alloy composition and growth velocity. Fig. 2(a) shows a pseudo binary phase diagram with constant solidus temperature T_m and liquidus temperature T_l reaching a minimum of 674 K at $La_{66}Al_{14}(Cu,Ni)_{20}$. It indicates that a pseudo-ternary eutectic reaction occurs at such a composition [12,13]. The liquidus lines at both sides are very steep with similar slopes of about 18 K/at.%. Fig. 2(b) shows the resultant microstructures as a function of alloy composition and growth velocity, in which five distinct morphologies were identified as

(1) E + La: Eutectic + La dendrites;
(2) E + C: Eutectic + intermetallic compounds;

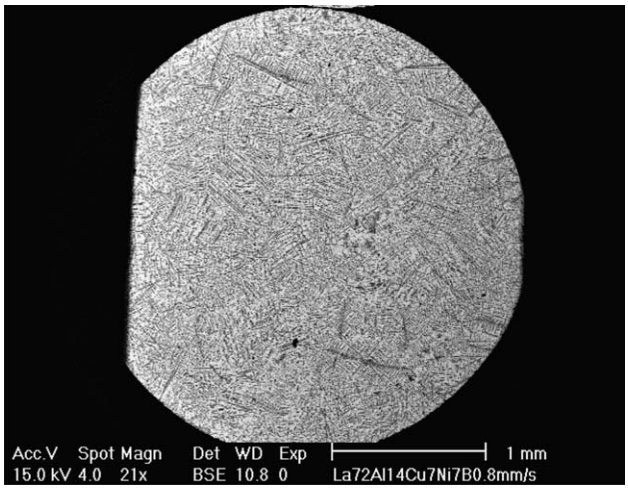

Fig. 1. SEM micrograph of the transverse section for a 3-mm rod sample prepared by Bridgman solidification.

Table 1
Typical morphologies of Bridgman solidified $La_xAl_{14}(Cu,Ni)_{86-x}$ alloys

V (mm/s)	$La_xAl_{14}(Cu,Ni)_{86-x}$ alloys							
	L59	L61	L62	L64	L66	L68	L72	L74
0.008	E + C		E + C		E		E + D	
0.1	E + C		E + C		E + D	E + D	E + D	E + D
0.2								A + D
0.3							E + D	A + D
0.4				E + D			A + D	
0.5	E		E	A + D	E + D		A + D	A + D
0.6	E	E	A	A + D	E + D	E + D		
0.8	E	A	A	A + D	E + D		A + D	A + D
1.0		A		A + D	A + D	A + D	A + D	A + D
1.1					A + D			
1.2					A + D	A + D		
1.3					A + D			
1.4					A + D			
2.0					A + D	A + D		
4.0					A + D			
4.8	E	A	A	A	A + D	A + D		

A: Amorphous; D: La dendrite; E: Eutectic; C: Compound.

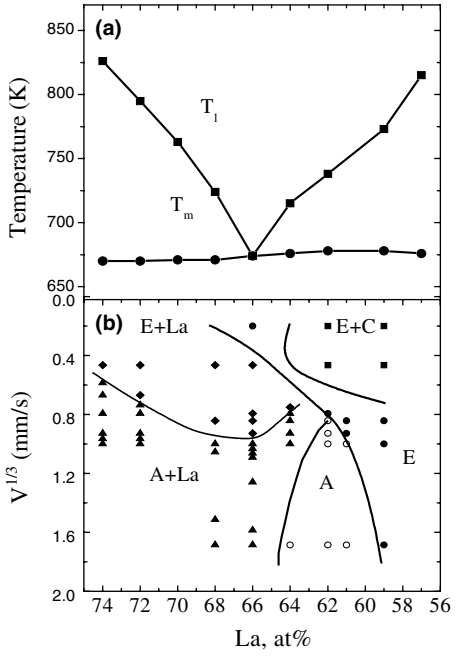

Fig. 2. (a) Phase diagram and (b) phase formation ranges for the $La_xAl_{14}[Cu,Ni]_{86-x}$ alloys. ●: eutectic (E); ○: amorphous (A); compound (C); ▲: A + La; ■: E + C; ◆: E + La.

(3) E: Eutectic;
(4) A + La: Amorphous + La dendrites;
(5) A: Amorphous.

It is noted that a skewed eutectic zone is seen towards the La-deficient portion and an amorphous zone with a narrow window of composition is less sensitive to growth velocity.

For the eutectic $La_{66}Al_{14}(Cu,Ni)_{20}$ alloy, with increasing growth velocity the microstructure evolved from eutectic (Fig. 3(a)), to a eutectic/dendrite composite (Fig. 3(b)), and then to an amorphous/dendrite composite (Fig. 3(c) and (d)). These results are in agreement with solidification of binary eutectic alloys with a skewed coupled zone [14]. In addition, with increase in growth velocity from 1.0 to 4.0 mm/s the volume fraction of La dendrites decreased from 35% to 28%. For the hypereutectic $La_{62}Al_{14}(Cu,Ni)_{24}$ alloy, as growth velocity increased the microstructure varied from a eutectic/compound composite at 0.008 mm/s (Fig. 4(a)), to full eutectic at 0.5 mm/s (Fig. 4(b)), and finally to a fully amorphous phase (Fig. 4(c)). Fig. 4(d) shows a transition from a eutectic/compound composite (bottom) to a featureless morphology of amorphous phase (top) when an abrupt change of growth velocity from 0.008 to 4.8 mm/s was applied in a growing $La_{62}Al_{14}(Cu,Ni)_{24}$ sample. Due to a short growth velocity range for eutectic formation of $La_{62}Al_{14}(Cu,Ni)_{24}$, eutectic growth was easily suppressed and instead a fully amorphous phase was obtained.

Fig. 5(a) shows the XRD patterns of $La_{66}Al_{14}(Cu,Ni)_{20}$ grown at different velocities. For samples obtained at growth velocities between 1.0 and 4.8 mm/s, their XRD patterns show crystalline peaks superimposed on an amorphous maximum, which implies the formation of a amorphous/crystalline composite structure. The crystalline phase was found in a dendritic form (Fig. 3(c)–(d)) and was identified as α-La [15]. On the other hand, for $La_{66}Al_{14}(Cu,Ni)_{20}$ grown below 0.8 mm/s only crystalline peaks were observed in the XRD patterns. Combined with Fig. 3(b), a composite structure composed of eutectic and La dendrites was obtained at growth velocities ranging from 0.1 to 0.8 mm/s. Fig. 5(b) shows the DSC heating curves of $La_{66}Al_{14}(Cu,Ni)_{20}$ grown at different velocities. As growth velocity

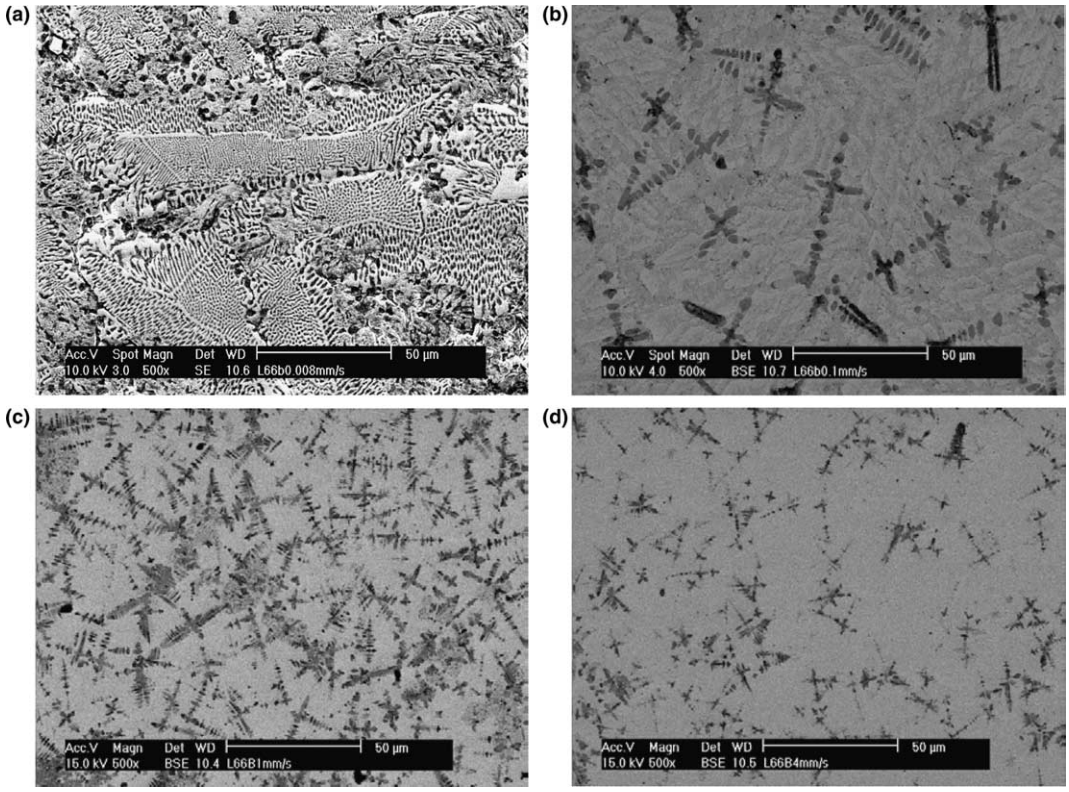

Fig. 3. SEM micrographs of $La_{66}Al_{14}(Cu,Ni)_{20}$ grown at: (a) 0.008 mm/s; (b) 0.1 mm/s; (c) 1 mm/s; (d) 4 mm/s.

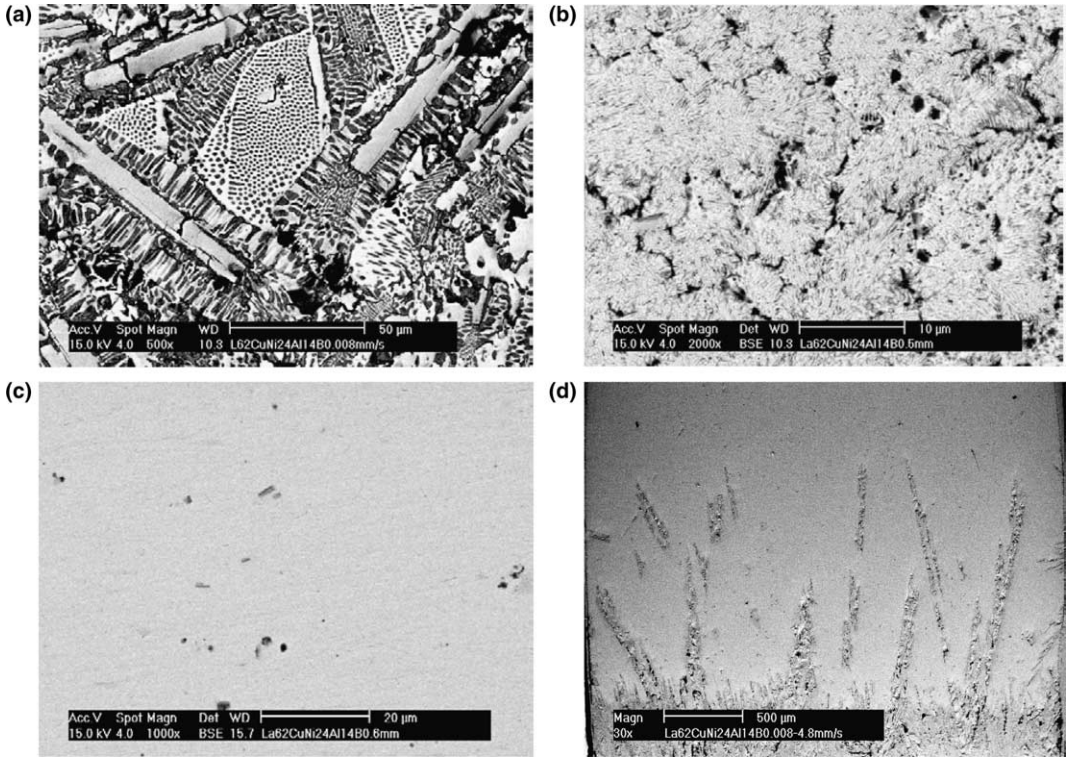

Fig. 4. SEM micrographs of $La_{62}Al_{14}(Cu,Ni)_{24}$ grown at: (a) 0.008 mm/s; (b) 0.5 mm/s; (c) 0.6 mm/s; (d) abrupt change from 0.008 to 4.8 mm/s.

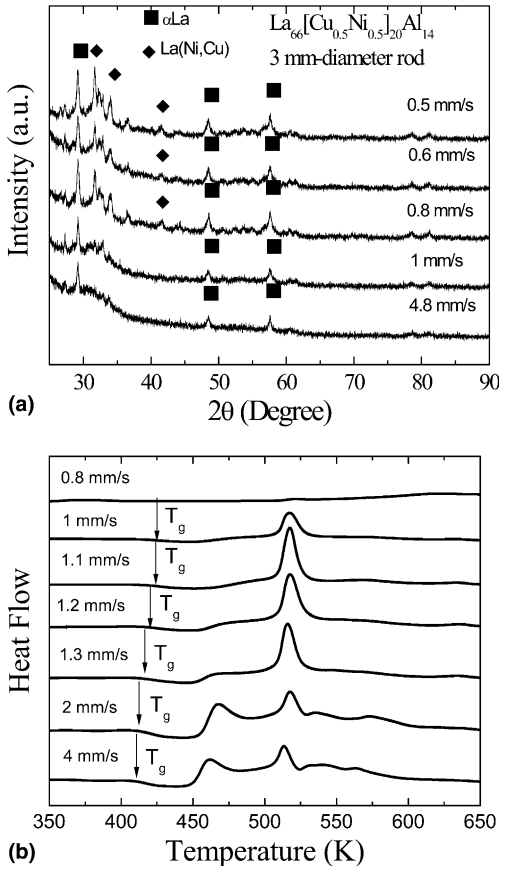

Fig. 5. (a) XRD patterns and (b) DSC heating curves of $La_{66}Al_{14}(Cu, Ni)_{20}$.

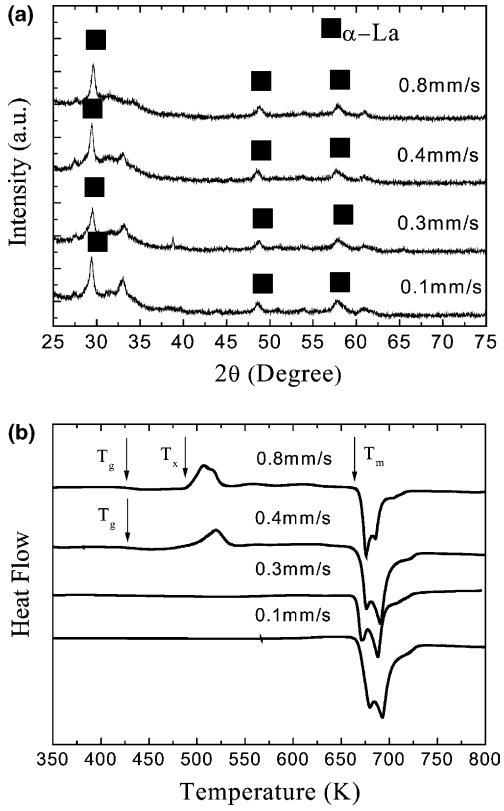

Fig. 7. (a) XRD patterns and (b) DSC heating curves of $La_{72}Al_{14}(Cu, Ni)_{14}$.

is higher than 1.0 mm/s, a distinct glass transition was noticed as well as subsequent crystallization, indicating the existence of an amorphous phase. The DSC results are in good agreement with those of SEM and XRD. In addition, the glass transition temperature, T_g, keeps almost constant at about 425 K for samples grown at various velocities. For $La_{66}Al_{14}(Cu, Ni)_{20}$ grown between 2.0 and 4.0 mm/s, the subsequent crystallization process involved a primary crystallization followed by a secondary crystallization. On the other hand, with decreasing growth velocity the primary crystallization peak was gradually reduced and finally vanished at a velocity of 1.1 mm/s. This is probably due to a higher onset crystallization temperature and therefore a larger T_x ($\Delta T_x = T_x - T_g$) for samples grown at lower velocities. Owing to the lack of amorphous phase, no obvious crystallization peak was observed for samples grown

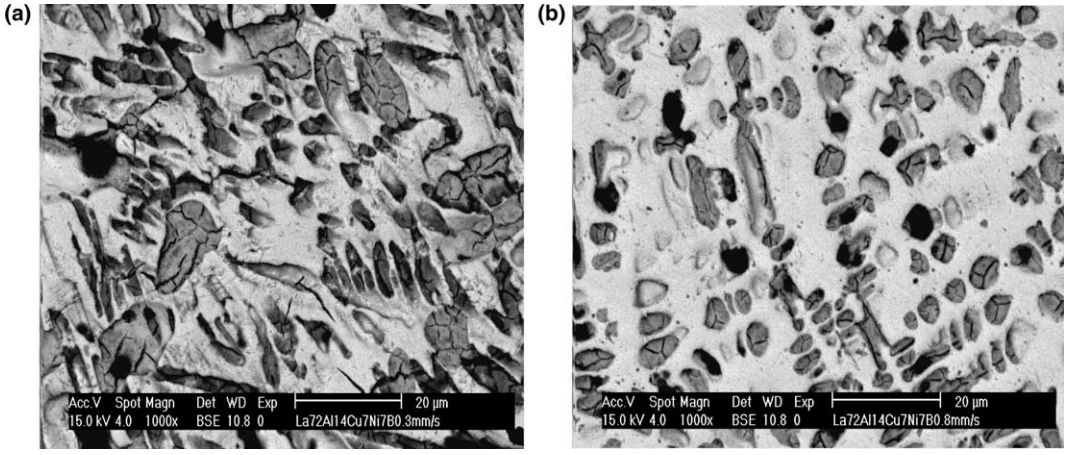

Fig. 6. SEM micrographs of $La_{72}Al_{14}(Cu, Ni)_{14}$ grown at: (a) 0.3 mm/s; (b) 0.8 mm/s.

below 0.8 mm/s, which is in agreement with the XRD patterns.

For the hypoeutectic $La_{72}Al_{14}(Cu,Ni)_{14}$ alloy, the critical growth velocity for the formation of amorphous phase is about 0.4 mm/s, below which a composite structure composed of eutectic and La dendrites formed (Fig. 6(a)) whereas above which an amorphous/dendrite composite was achieved (Fig. 6(b)). As growth velocity increased from 0.1 to 0.8 mm/s, the volume fraction of La dendrites firstly increased to a maximum of 73% at 0.3 mm/s, and then decreased to 51% at 0.8 mm/s. The interphase spacing (λ) of the eutectic structure decreased from 0.13 to 0.08 μm as growth velocity increased from 0.1 to 0.3 mm/s. Fig. 7 shows the XRD patterns and DSC heating curves of $La_{72}Al_{14}(Cu,Ni)_{14}$ grown at different velocities, which prove the formation of eutectic/dendrite and amorphous/dendrite composites at low and high growth velocities, respectively.

3.2. Mechanical properties

As identified from Fig. 2(b), four composite structures were obtained in $La_xAl_{14}(Cu,Ni)_{86-x}$ alloys, i.e., eutectic/dendrite, amorphous/dendrite, eutectic/compound and eutectic. Since the existence of intermetallic compounds can lead to embrittlement and eventually failure of materials without plastic deformation, in the present study, eutectic/dendrite and amorphous/dendrite composites were chosen for the characterization of mechanical properties. A series of uniaxial compression tests were conducted on $La_{66}Al_{14}(Cu,Ni)_{20}$ and $La_{72}Al_{14}(Cu,Ni)_{14}$ alloys. For simplicity, the characterized samples are denoted by A1, A2, A3, A4, B1 and B2, and are summarized in Table 2 together with their morphologies and compressive properties.

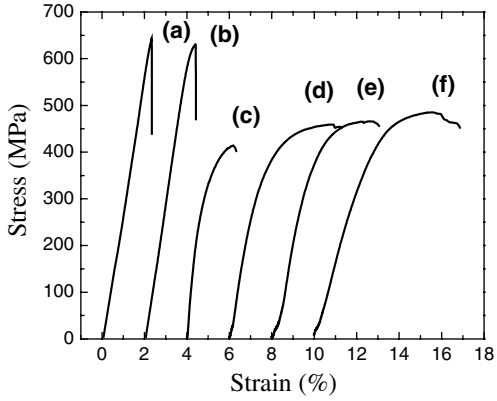

Fig. 8. Compressive stress–strain curves of samples: (a) A1; (b) A2; (c) B1; (d) B2; (e) A4; (f) A3.

Fig. 8 shows the compressive true stress–strain curves of $La_{66}Al_{14}(Cu,Ni)_{20}$ and $La_{72}Al_{14}(Cu,Ni)_{14}$. The amorphous/dendrite composites of $La_{66}Al_{14}(Cu,Ni)_{20}$ show linear elastic behaviour (Fig. 8(a) and (b)) with fracture strength of 643 and 630 MPa for A1 and A2, respectively. A1 failed being quasi-brittle almost without any macroscopic plasticity at elastic strain of about 2.3%, whereas a small amount of plastic strain of about 0.4% was achieved for A2 due to a slightly higher volume fraction (35%) of La dendrites. The volume fraction (28%) of La dendrites for A1 is not high enough to distribute the shear bands uniformly and therefore results in poor plasticity [7,16]. In addition, both A1 and A2 exhibit a similar Young's modulus of about 28 GPa, which

Table 2
Typical compressive properties of Bridgman solidified $La_xAl_{14}(Cu,Ni)_{86-x}$ alloys

Specimens		V (mm/s)	Volume fraction (%)	$\sigma_{0.2}$ (MPa)	σ_f (MPa)	ε_E (%)	ε_p (%)	Microstructure
L66	A2	1.0	35		630	2.3	0.4	A + D
		1.1	35		615		0.2	A + D
		1.2	34		656		0.2	A + D
		1.3	32		662		0.4	A + D
		2.0	31		581		0	A + D
	A1	4.0	28		643	2.3	0	A + D
L72	B1	0.1	59	280	402	0.6	1.2	E + D
	B2	0.3	61	305	452	1.4	3.2	E + D
	A4	0.4	60	330	455	1.6	2.8	A + D
		0.5	59	420	423		0.6	A + D
	A3	0.8	59	380	452	2.5	3.8	A + D
		0.9	60	385	470		2.1	A + D
		1.0	60	400	471		1.2	A + D
L74		0.1	58		420		0	E + D
		0.2	65		440		0	A + D
		0.3	63		463		0	A + D
		0.5	63	410	504		1.9	A + D
		0.8	63	320	479		4.7	A + D
		0.9	62	450	487		0.4	A + D
		1.0	54	370	450		0.6	A + D

indicates that the Young's modulus is not sensitive to the variation of volume fraction of La dendrites. On the other hand, the amorphous/dendrite and eutectic/dendrite composites of $La_{72}Al_{14}(Cu,Ni)_{14}$ exhibited initial elastic deformation followed by plastic deformation before fracture (Fig. 8(c)–(f)). The fracture strength is measured to be 402, 452, 455 and 452 MPa for B1, B2, A4 and A3, respectively. As compared with A1 and A2 of $La_{66}Al_{14}(Cu,Ni)_{20}$, A3 and A4 of $La_{72}Al_{14}(Cu,Ni)_{14}$ showed lower fracture strength but much improved ductility (plastic strain of 3.8% and 2.8% for A3 and A4, respectively) due to their higher volume fractions of La dendrites. For eutectic/dendrite composites of B1 and B2, higher fracture strength of 452 MPa for B2 is due to a finer eutectic spacing whereas larger plastic strain of 3.2% for B2 is the outcome of a higher volume fraction of La dendrites.

Fig. 9(a) shows the typical fracture angles between the compression stress axis and the shear plane of the amorphous/dendrite. The fracture angles are in the range of 41–44° for amorphous/dendrite samples, which are higher than the previously reported 27–32° for bulk metallic glass composites with ductile dendrites [17]. Fig. 9(b) shows the La dendrites on the fracture surface. Two kinds of fracture regions were observed (Fig. 9(c)), namely, deep vein patterns at the La dendrites (the inset of Fig. 9(c)), and flat fracture surface in the amorphous matrix. In addition, the fracture surfaces of the amorphous/dendrite composites exhibited fracture surface remelting (Fig. 9(d) and (e)), which is in good agreement

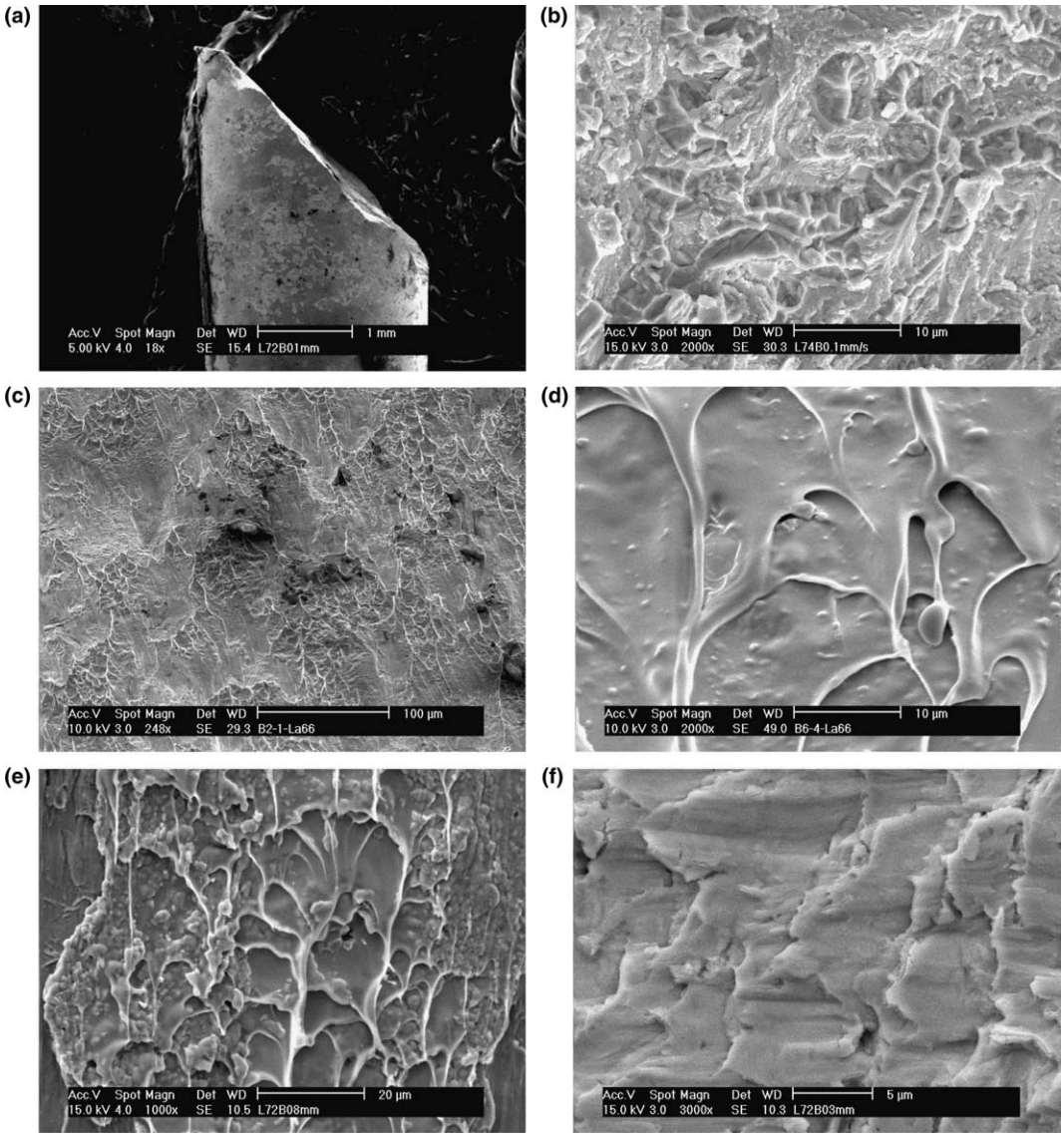

Fig. 9. Typical compression fracture of: (a) fracture angle of $La_{72}Al_{14}(Cu,Ni)_{14}$ grown at 0.1 mm/s; (b) fracture surface of $La_{74}Al_{14}(Cu,Ni)_{12}$ grown at 0.1 mm/s; (c) fracture surface of $La_{66}Al_{14}(Cu,Ni)_{20}$ grown at 1.1 mm/s; (d) fracture surface of $La_{66}Al_{14}(Cu,Ni)_{20}$ grown at 4 mm/s; (e) fracture angle of $La_{72}Al_{14}(Cu,Ni)_{14}$ grown at 0.8 mm/s; (f) fracture angle of $La_{72}Al_{14}(Cu,Ni)_{14}$ grown at 0.3 mm/s.

with previous studies [16,17]. The occurrence of fracture surface remelting implies large elastic strain energy and a high local temperature increase produced during deformation. The increased local temperature may be higher than T_g or T_l [18]. For eutectic/dendrite composites, the fracture surface shows flake-like patterns as shown in Fig. 9(f). There is no obvious fracture surface remelting, which indicates a different fracture mechanism for eutectic/dendrite composites.

4. Discussion

4.1. Skewed eutectic coupled zone and microstructure control

Instead of eutectic $La_{66}Al_{14}(Cu,Ni)_{20}$, the La based La–Al–(Cu, Ni) pseudo ternary system exhibits its best glass forming ability (GFA) at an off-eutectic composition, $La_{62}Al_{14}(Cu,Ni)_{24}$ [12]. This phenomenon has been ascribed to the formation of a skewed eutectic coupled zone that is towards the faceted phase La(Cu, Ni) [12,13,15]. Six distinct morphologies were predicted in the La based La–Al–(Cu, Ni) system, that is, eutectic + La dendrites, eutectic, eutectic + compounds, amorphous + La dendrites, amorphous, and amorphous + compounds [12]. For alloy compositions studied in the present paper, the absence of amorphous + compounds is possibly due to its narrow temperature formation range or a low T_g.

Although a fully amorphous phase is easily achieved at an off-eutectic composition, its poor plastic strain has limited its applications. In addition, at low growth velocities the presence of a brittle compound phase in an off-eutectic alloy is apt to result in the failure of materials without plastic strain. To achieve optimized mechanical properties, it is obvious that one should make more efforts to study the hypoeutectic alloys, so as to produce a composite structure composed of a certain amount of ductile La dendrites. As shown in Figs. 2 and 6, for eutectic and hypoeutectic alloys a transition from a eutectic/dendrite to an amorphous/dendrite composite was observed as growth velocity increased. The resultant microstructures mainly depend on competitive growth of the constituent phases, which can be interpreted by comparing their growth temperatures as a function of growth velocity. For the present La based eutectic and hypoeutectic alloys, Fig. 10 shows schematic diagrams on the dependence of growth temperatures on growth velocity for the four constituent phases, namely, eutectic, La dendrite, compound and amorphous. It should be pointed out that the eutectic growth temperature is independent of alloy composition, whereas T_g is independent of growth velocity. With increasing growth velocity, three critical growth velocities can be identified as V_1, $V_{E/A}$ and $V_{La/A}$. They represent transitions from fully eutectic to eutectic + La dendrites, from eutectic + La dendrites to amorphous + La dendrites, and from amorphous + La dendrites to a fully amorphous phase, respectively. With increasing La content from eutectic $La_{66}Al_{14}(Cu,Ni)_{20}$ to hypoeutectic $La_{72}Al_{14}(Cu,Ni)_{14}$, the growth temperature of La dendrites gradually increases, which results in a decrease of V_1 and an increase of $V_{La/A}$. For the $La_{72}Al_{14}(Cu,Ni)_{14}$ alloy, a fully eutectic structure was not observed since the growth temperature of La dendrites is higher than that of eutectic at any growth velocity and V_1 is therefore nearly zero. On the other hand, a fully amorphous phase is not achieved in the three alloys because $V_{La/A}$ is higher than the imposed maximum growth velocity of 4.8 mm/s. In addition, it has been reported that with increasing La content from $La_{66}Al_{14}(Cu,Ni)_{20}$ to $La_{72}Al_{14}(Cu,Ni)_{14}$, T_g gradually increased from 409.23 to 426.72 K [19] and therefore led to a decrease of $V_{E/A}$, which is in good agreement with Fig. 2(b). That is, as La content increased the critical growth velocity decreased for the transition from a eutectic/dendrite to an amorphous/dendrite composite.

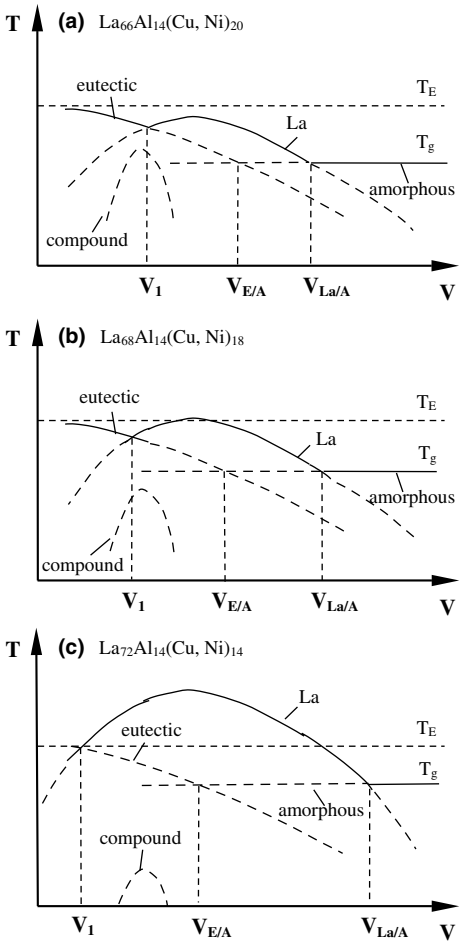

Fig. 10. Schematic diagrams of the dependence of growth temperatures on growth velocity of the four constituent phases for: (a) $La_{66}Al_{14}(Cu,Ni)_{20}$; (b) $La_{68}Al_{14}(Cu,Ni)_{18}$; (c) $La_{72}Al_{14}(Cu,Ni)_{14}$.

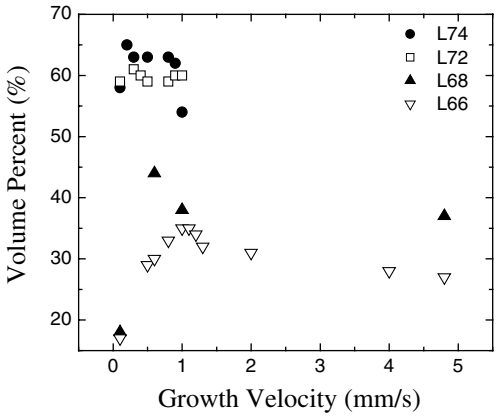

Fig. 11. Dependence of volume fraction of La dendrites on growth velocity.

Apart from the transition from a eutectic/dendrite to an amorphous/dendrite composite, the control of ductile La dendrites is essential for improvement of plastic strain. Fig. 11 shows the dependence of volume fraction of dendrites on growth velocity. With increasing growth velocity, the volume fraction gradually increased and reached a maximum at a critical growth velocity such as 1 mm/s for $La_{66}Al_{14}(Cu,Ni)_{20}$, after which it levelled off. The effects of growth velocity on volume fraction of dendrites can be qualitatively elucidated by nucleation and growth of dendrites. At lower growth velocities, the formation of La dendrites is mainly governed by diffusion-controlled growth once nucleation of La phase has completed. The increase in growth velocity leads to the increase of nucleation density as well as the decrease of local solidification time. Although the decrease of local solidification time has reduced diffusion-controlled growth of dendrites, the increase of nucleation density contributes to volume fraction to a larger extent and therefore results in the increase of volume fraction until it reaches a maximum at a critical growth velocity. However, above the critical value, the contribution from the increase of nucleation density is not high enough to compensate the reduction due to the limited diffusion-controlled growth. In addition, at higher growth velocities the supercooled liquid transformed into an amorphous phase has led to the decrease of atomic diffusivity, which limits the growth of dendrites. Therefore, above a critical growth velocity a decrease in volume fraction of dendrites is inevitable.

4.2. Correlation between microstructures and mechanical properties

Bulk metallic glasses generally exhibit high fracture strength and high elastic limit but low ductility. For instance, fracture strength of the fully amorphous La alloy is over 561 MPa (no yield) [19], which is about eight times the value of 75 MPa (yield strength) for the crystalline La [19]. On the other hand, no plastic strain was observed for the fully amorphous La alloy in comparison with that of over 18% for the crystalline La [19]. It is necessary to keep a proper balance between fracture strength and plastic strain to satisfy the criteria of practical applications. Apart from macro and micro defects, mechanical properties are mainly determined by the resultant microstructures that are characterized by the constituent phases and their characteristic length scales. The present section will be mainly focused on the dependence of mechanical properties on volume fraction of the constituent phases.

Obviously, the strength of the composites is attributable to the amorphous or eutectic matrix, whereas the dendrites act as obstacles to limit the excessive deformation in the localized shear bands and contribute to the plasticity. Any variation in alloy composition or solidification condition may lead to the alteration of solidification behavior of the constituent phases, and therefore affect its resultant microstructures as well as mechanical behavior to a certain extent. For La based alloys, Lee et al. [19] have made some efforts to control the volume fraction of ductile La dendrites by means of adjusting alloy composition, so as to optimize mechanical properties. With increasing La content from $La_{62}Al_{14}(Cu,Ni)_{24}$ to $La_{85}Al_{14}(Cu,Ni)_{1}$, volume fraction of La dendrites gradually increased up to 53%, which led to an increase of compressive plastic strain from zero to 6% without significant loss of strength. Such a combination of mechanical properties has an advantage over that of a fully amorphous alloy for the practical applications. For samples prepared by Bridgman solidification, Fig. 12 shows the dependence of fracture strength and plastic strain on volume fraction of La dendrites. The increase in volume fraction of La dendrites resulted in a decrease of fracture strength, which obeys the mixture law. Compared with samples prepared by copper mould casting [19] (open circles in Fig. 12), the Bridgman solidified samples seem to exhibit a higher fracture strength at a given dendritic volume fraction. It may be due to the formation of more homogeneous microstructure in samples prepared by Bridgman solidification. From Fig. 12(a), it is noted that the variation of fracture strength in dendritic volume fraction is similar for samples prepared by both Bridgman solidification and copper mould casting (around 5 MPa per 1% change of dendritic volume fraction). In addition, no abrupt change of fracture strength was observed as the matrix was transformed from eutectic to an amorphous phase. It seems that both matrices have an equivalent contribution to the strength. On the other hand, with increasing volume fraction of La dendrites the plastic strain has shown an exponential increase for samples prepared by both Bridgman solidification and copper mould casting. It is noted that the critical volume fraction for the sharp increase of plastic strain for Bridgman solidified samples

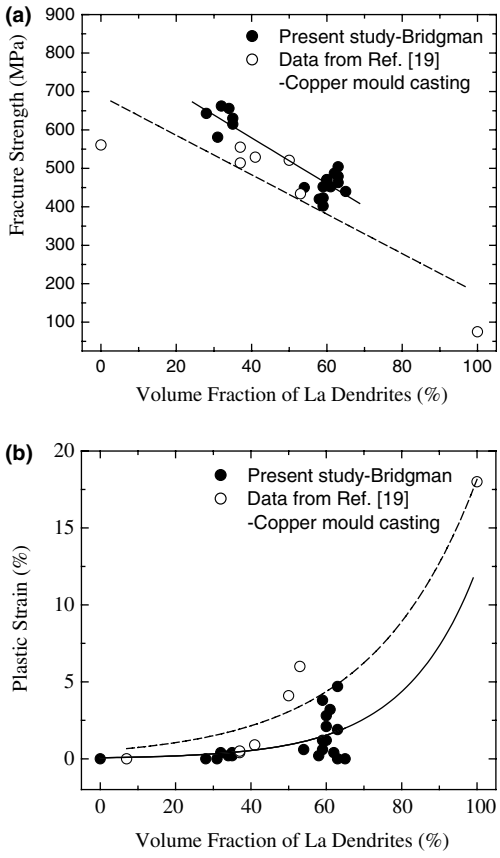

Fig. 12. Dependence of (a) fracture strength and (b) plastic strain on volume fraction of La dendrites. Closed circles are data of the present study whereas open circles are data from Ref. [19].

is around 60%, which is higher than that of 40% for copper mould casting samples [19]. The difference is possibly due to other factors such as the size of dendrites, interdendritic spacing and solute solubility in the dendrites, which are not our present focus and on which further investigations are needed. From the above discussion based on Fig. 12, it can be preliminarily concluded that in order to achieve high strength and good ductility, a slow variation of fracture strength and a low critical dendritic volume fraction are expected.

5. Conclusions

$La_xAl_{14}(Cu,Ni)_{86-x}$ alloys were studied by Bridgman solidification at growth velocities ranging from 0.008 to 4.8 mm/s. Five distinct morphologies were identified as eutectic, amorphous, eutectic + compound, amorphous + dendrite, and eutectic + dendrite. Hypoeutectic alloys are preferred to produce amorphous/dendrite and eutectic/dendrite composites with optimised mechanical properties since the eutectic coupled zone is skewed towards the compound phase. As the La content increased, the critical growth velocity decreased for the transition from a eutectic/dendrite to an amorphous/dendrite composite. The effects of growth velocity on volume fraction of dendrites were also qualitatively elucidated by nucleation and growth of dendrites. In addition, with increasing volume fraction of La dendrites, the compressive properties of the composites exhibited decreased fracture strength and improved ductility. Therefore, the mechanical properties can be optimised through alloy composition design and well-controlled solidification processing.

Acknowledgements

The authors acknowledge the financial support of Singapore-MIT Alliance (SMA), and one of the authors Y.Z. is grateful for the technical assistance of Dr. M.L. Lee, and the helpful discussion with Prof Z.Q. Sun.

References

[1] Inoue A, Zhang T, Masumoto T. Mater Trans JIM 1989;30:956.
[2] Johnson WL. MRS Bull 1999;24:42.
[3] Li Y, Jones H, Davies HA. Scripta Metall 1992;26:1371.
[4] Wang WH, Dong C, Shek CH. Mater Sci Eng R 2004;44:45.
[5] Lu ZP, Liu CT. J Mater Sci 2004;39:3965.
[6] Hays CC, Kim CP, Johnson WL. Phys Rev Lett 2000;84:2901.
[7] Szuecs F, Kim CP, Johnson WL. Acta Mater 2001;49:1507.
[8] Kühn U, Eckert J, Mattern N, Schultz L. Appl Phys Lett 2002;80:2478.
[9] Fan C, Ott RT, Hufnagel TC. Appl Phys Lett 2002;81:1020.
[10] He G, Löser W, Eckert J, Schultz L. J Mater Res 2002;17:3015.
[11] He G, Eckert J, Löser W. Acta Mater 2003;51:1621.
[12] Tan H, Zhang Y, Ma D, Feng YP, Li Y. Acta Mater 2003;51:4551.
[13] Ma D, Tan H, Zhang Y, Li Y. Mater Trans 2003;40:2007.
[14] Kurz W, Fisher DJ. Int Met Rev 1979;5–6:177.
[15] Tan H, Zhang Y, Li Y. Intermetallics 2002;10:1203.
[16] Eckert J, Kühn U, Mattern N, He G, Gebert A. Intermetallics 2002;10:1183.
[17] Zhang ZF, He G, Eckert J, Schultz L. Phys Rev Lett 2003;94:045505.
[18] Liu CT, Healtherly L, Easton DS, Carmichael CA, Schneibel JH, Chen CH, et al. Metall Mater Trans A 1998;29:1811.
[19] Lee ML, Li Y, Schuh CA. Acta Mater 2004;52:4121.